Disinhibitory circuitry gates associative synaptic plasticity in olfactory cortex

Martha Canto-Bustos[1,2], F. Kathryn Friason[1,2], Constanza Bassi[1] and Anne-Marie M. Oswald[1,2,3]*

[1]Department of Neuroscience, [2]Center for the Neural Basis of Cognition,

University of Pittsburgh, Pittsburgh, PA, United States, 15213

Corresponding Author:
Anne-Marie M. Oswald
Associate Professor
Department of Neuroscience
University of Pittsburgh
A210 Langley Hall
Pittsburgh, PA, 15260

[3]Current Address
Department of Neurobiology
Neuroscience Institute
University of Chicago
Abbott Memorial Hall
947 East 58th St. MC0928
Chicago, IL, USA, 60637
amoswald@uchicago.edu

Abstract

Inhibitory microcircuits play an essential role in regulating cortical responses to sensory stimuli. Interneurons that inhibit dendritic or somatic integration in pyramidal neurons act as gatekeepers for neural activity, synaptic plasticity and the formation of sensory representations. Conversely, interneurons that specifically inhibit other interneurons can open gates through disinhibition. In the rodent piriform cortex, relief of dendritic inhibition permits long-term potentiation (LTP) of the recurrent synapses between pyramidal neurons (PNs) thought to underlie ensemble odor representations. We used an optogenetic approach to identify the inhibitory interneurons and disinhibitory circuits that regulate LTP. We focused on three prominent inhibitory neuron classes- somatostatin (SST), parvalbumin (PV), and vasoactive intestinal polypeptide (VIP) interneurons. We find that VIP interneurons inhibit SST interneurons and promote LTP through subthreshold dendritic disinhibition. Alternatively, suppression of PV-interneuron inhibition promotes LTP but requires suprathreshold spike activity. Thus, we have identified two disinhibitory mechanisms to regulate synaptic plasticity during olfactory processing.

Throughout the cortex, the response properties of individual neurons as well as coordinated ensemble activity are refined by sensory experience. One underlying feature of experience-dependent plasticity is long-term changes in synaptic strength within cortical circuits. While the mechanisms underlying excitatory synaptic plasticity have been extensively studied (Abbott and Nelson 2000, Malenka and Bear 2004), less is known about the role cortical circuitry plays in gating changes in synaptic strength. Inhibitory interneurons regulate both dendritic integration and neural activity, two major factors in synaptic plasticity. Thus, inhibitory circuits can play a key role in the enhancement of synaptic connections (Artinian and Lacaille 2018, Lucas and Clem 2018). In this study, we elucidate the inhibitory and disinhibitory circuit motifs that gate synaptic plasticity at recurrent excitatory synapses in the olfactory cortex.

The anterior piriform cortex (APC) processes olfactory information, and performs both sensory and associative cortical functions. Located two synapses from the periphery; the APC is a primary cortical area representing odor inputs. Olfactory receptor neurons in the nose project to Mitral and Tufted (M/T) neurons in the olfactory bulb (OB)(Mombaerts, Wang et al. 1996). M/T neurons then project directly to APC and synapse with pyramidal neurons (PNs)(Haberly and Price 1977). Unlike other primary sensory cortices, APC lacks a topological representation of odor identity. M/T axons project diffusely and randomly (Sosulski, Bloom et al. 2011, Igarashi, Ieki et al. 2012) to activate distributed neural ensembles (Illig and Haberly 2003, Rennaker, Chen et al. 2007, Stettler and Axel 2009). Distributed odor representations are further supported by uniform intracortical excitatory connectivity across the APC (Franks, Russo et al. 2011). It is postulated that odor-specific ensembles are constructed by strengthening excitatory synapses between pyramidal neurons co-activated by odor components (Haberly 2001, Wilson and Sullivan 2011). In support of this hypothesis, intracortical synapses between PNs are strengthened following odor learning *in vivo* (Saar, Grossman et al. 2002) and through pairing of afferent and intracortical stimulation *in vitro* (Kanter and Haberly 1993, Johenning, Beed et al. 2009). Hence, APC circuitry also supports early stage, associative odor processing.

The APC is an ideal structure for investigating the circuit and synaptic plasticity mechanisms that underlie sensory representations. PNs receive compartmentalized excitatory inputs on their apical dendrites from two distinct fiber tracts. M/T cells afferents synapse distally, while PN axons form a proximal intracortical fiber tract (Haberly and Price 1977, Haberly and Price 1978). Co-activation of afferent and intracortical fiber tracts strengthens intracortical synapses onto PNs through NMDA receptor (R) dependent, associative LTP (Kanter and Haberly 1993). Further, NMDAR EPSPs and associative LTP induction are facilitated by dendritic disinhibition by $GABA_A$ receptor antagonists (Kanter and Haberly 1993, Kanter, Kapur et al. 1996). While these studies suggest interplay between dendritic inhibition and disinhibition gates LTP induction at intracortical synapses, the inhibitory circuitry involved has not been identified.

Olfactory stimuli recruit both feedforward and recurrent inhibition onto PNs in APC (Poo and Isaacson 2009, Poo and Isaacson 2011). Feedforward inhibition is comparatively weak and diminishes with high frequency stimulation of the afferent pathway, whereas recurrent inhibition is strong, and increases with stimulation through synaptic facilitation and PN recruitment (Stokes and Isaacson 2010, Suzuki and Bekkers 2010a, Large, Vogler et al. 2016). Recurrent inhibition is mediated by inhibitory interneurons that express somatostatin (SST-INs) or parvalbumin (PV-INs) (Stokes and Isaacson 2010, Suzuki and Bekkers 2010a, Suzuki and Bekkers 2010b, Large, Kunz et al. 2016). SST-INs inhibit PN apical dendrites proximal to the soma, and are optimally located to regulate plasticity of intracortical synapses (Suzuki and Bekkers 2010b, Large, Kunz et al. 2016). PV-INs regulate spike activity and could also impact LTP through backpropagation (Johenning, Beed et al. 2009). A third class of interneurons- vasoactive intestinal polypeptide interneurons (VIP-INs); inhibit SST and PV-INs and could disinhibit pyramidal neurons (Lee, Kruglikov et al. 2013, Pfeffer, Xue et al. 2013, Karnani, Jackson et al. 2016). VIP-INs are a prominent in APC (Suzuki and Bekkers 2010b) but their inhibitory connections and function are unknown. We investigated the connectivity and

functional roles of SST, PV and VIP-INs in APC. We find that activation of VIP-INs as well as inactivation of SST-INs or PV-INs promote LTP of intracortical synapses. VIP-INs strongly inhibit SST-INs during LTP induction, but only weakly inhibit PV-INs and PNs. We provided evidence for two disinhibitory circuit mechanisms in APC that promote LTP- one acts in the subthreshold through a VIP-SST-PN pathway; and the other through increases in suprathreshold activity and PV-IN inhibition.

Methods:

Mice: VIP-Cre *(*B6:Viptm1(cre)Zjh/J) , SST-Cre (B6:Sst<tm2.1(cre)Zjh>/J) and PV-Cre mice express cre-recombinase (Taniguchi, He et al. 2011). These mice were crossed with Ai32 mice (B6;129S-Gt ROSA)26Sortm32 (CAG-COP4*H134R/EYFP)Hze/J) to express channelrhodopsin (ChR2) or Ai35 mice (B6.129S-*Gt(ROSA*)26Sortm35.1(*CAG- aop3/GFP)Hze*/J) to express archaerhodopsin (Arch) (Madisen, Mao et al. 2012). All mice are from Jackson Laboratory. All animals were bred, handled and treated in manner that was evaluated and approved by the Animal Care and Use Committee at the University of Pittsburgh IACUC, protocol #17070877.

Slice preparation: APC brain slices were prepared from mice aged P19-35. The mice were anesthetized with isoflurane and the brain was removed and immersed in ice cold oxygenated (95% O_2-5% CO_2) ACSF (in mM: 125 NaCl, 2.5 KCl, 25 $NaHCO_3$, 1.25 NaH_2PO_4, 1.0 $MgCl_2$, 25 Dextrose, 2.5 $CaCl_2$) (all chemicals from Sigma, USA unless otherwise stated). Parasagittal slices (300 μm) were cut on a vibratome (Leica Biosystems) in ice-cold ACSF. The slices were transferred to warm ACSF (37°C) for 30 min, then 20-22°C for 1 hour, and recorded at 31-35°C.

Electrophysiology: Recordings were performed using a MultiClamp 700B amplifier (Molecular Devices, Union City, CA). Data were low pass filtered (4 kHz) and digitized at 10 kHz using an ITC-18 (Instrutech) controlled by custom software (Recording Artist, https://bitbucket.org/rgerkin/recording-artist) written in IgorPro (Wavemetrics). Recording

pipettes (4-10 MΩ) were pulled from borosilicate glass (1.5 mm, outer diameter) on a Flaming/Brown micropipette puller (Sutter Instruments). The series resistance (<20 MΩ) was not corrected. For PSPs the intracellular solution consisted of (in mM) 130 K-gluconate, 5 KCl, 2 $MgCl_2$, 4 ATP-Mg, 0.3 GTP, 10 HEPES, and 10 phosphocreatine, 0.05% biocytin. For IPSC recordings, Qx-314 was added to the K-gluconate internal (holding potential 0 mV) or Cs-Glu-Qx solution was used (in mM, 130 Cs-Gluconate, 5 KCl, 2 $MgCl_2$, 4 Mg-ATP, 0.3 GTP, 10 HEPES, 10 Phosphocreatine, 1 Qx-314, holding potential +30 mV). Neurons were visualized using infrared-differential interference contrast microscopy (IR-DIC, Olympus). For all recorded neurons, subthreshold response properties were obtained using a series of hyperpolarizing and depolarizing current steps (-50 pA to 50 pA, 1 s duration). Neural identity was confirmed post hoc using intrinsic properties and biocytin fills.

LTP induction: Electrical stimulation was delivered using concentric bipolar electrodes (FHC). The electrodes were placed in the LOT (L1a) and the L1b/L2 border. Stimuli (100 μs pulse width) were delivered through a stimulus isolation unit. Theta burst stimulation (TBS) of L1a consisted of 10 bursts of 4 pulses (100 Hz) delivered at 250 ms intervals (Kanter and Haberly 1993). TBS stimulation intensity was set near spike threshold for the recorded neuron. L1b was stimulated with a single weak pulse delivered between the 3rd and 4th pulse of each burst. Stimulation intensity was <30% of the maximum subthreshold EPSP (~1-6 mV). Pre and post induction test pulses were delivered to L1b every 30 s. Baseline was collected for ~5 min and LTP was induced within 10 min of patching the neuron. Series resistance and input resistance were monitored throughout and neurons with deviations greater than +20% from baseline were excluded from analysis.

Optogenetic Stimulation: Shutter controlled full field stimulation with blue (473 nm) or green (520 nm) light (Prior) was delivered through the epifluorescence pathway of the microscope (Olympus) using a water-immersion objective (40x). Light intensity (5-10W) was adjusted to

induce spike responses (ChR2 activation) or spike suppression (Arch inactivation). Light pulse duration varied by experiment as indicated.

Statistics: All data is presented as mean ± SE. Statistical tests were performed using two tailed, one or two-sample, paired or unpaired Student's t-test as appropriate. Since no pilot studies were conducted, sample sizes were initially determined based on sample sizes and mean data from previous similar studies. All major findings of this study have a power greater than 80% at a 5% level of significance. In cases of small sample sizes (<10) non-parametric tests were used, including the Mann-Whitney U-test (MWU) for unpaired data and the Wilcoxon Signed Ranks test (WSR) for paired data. For multiple comparisons we used ANOVA with post hoc Tukey Test (ANOVA).

Results:

We investigated the roles of SST, PV and VIP-INs, in gating associative LTP at intracortical excitatory synapses onto PNs. Afferent input to PNs arrives via L1a on distal L2 PN dendrites, while the intracortical fiber tract (L1b) is proximal (**Fig 1A**). L1a and L1b were easily identified under IR-DIC and independently stimulated using bipolar electrodes. Associative LTP is induced by pairing L1a and L1b stimulation using a theta burst stimulation (TBS) protocol (Kanter and Haberly 1993) consistent with respiration coupled M/T spike frequencies (Kepecs, Uchida et al. 2007, Carey and Wachowiak 2011). Briefly, strong TBS of L1a was paired with weak, single pulse stimulation of L1b (see methods, **Fig 1A**). This L1a+L1b pairing is hereafter denoted *induction*. L1a-TBS evoked low PN firing rates (FR, 0-5 Hz) and L1b EPSPs ranged from 1-6 mV. Pre and post induction, L1b stimulation was delivered every 30 s. To avoid drift in recording integrity, potentiation was quantified as the average L1b EPSP amplitude 25-30 min following induction versus average baseline EPSP amplitude (5 min prior to induction). However, potentiation typically lasted for the duration of recording (~60 min). Both raw and normalized (to

baseline) EPSP amplitude and area were analyzed. PNs with input resistances or membrane potentials varying more than 20% from baseline were excluded.

Disinhibition of PN dendrites promotes LTP

With inhibition intact, the induction protocol did not induce LTP of L1b synapses (in mV, pre: 2.8 ± 0.5, post: 2.9 ± 0.5, p: 0.671, paired t-test, n=12 PNs, **Fig 1B,C, left**). Likewise, normalized EPSP amplitude and area did not differ significantly from 1 (Amplitude: 1.0 ± 0.1, p: 0.48; Area: 1.2 ± 0.1, p: 0.09, one sample t-test, **Fig 1C, right**). To confirm that dendritic disinhibition promotes LTP, we focally applied the $GABA_A$ receptor antagonist, Gabazine (GZ, 20 μM), to L1b (schematic, **Fig 1D1**). In this case, induction significantly enhanced EPSPs (mV, Pre: 1.1 ± 0.2, Post: 3.5 ± 1.1, p: 0.048 paired t-test, n=**Fig 1B,D**). Normalized EPSP area was significantly greater than 1 (Area: 4.8 ± 1.7, p: 0.047, one sample t-test). However, normalized amplitude did not significantly differ from 1 (3.4 ± 1.7, p: 0.058) due to a strongly potentiated outlier. Absent this point, normalized amplitude is significantly greater than 1 (2.4 ± 0.4, p: 0.005, **red ****, **Fig. 1D3, Supplemental Table 1**). In a subset of slices from SST-ChR2 mice, GZ application to L1b blocked optically evoked SST-mediated inhibition (Large, Kunz et al. 2016) (n=5, **Fig 1E**) and promoted LTP. This suggests that SST-INs provide dendritic inhibition and may modulate synaptic plasticity.

Inactivation of SST-INs promotes LTP

To confirm a role for SST-mediated inhibition in gating synaptic plasticity, we optically inactivated SST-INs in slices from SST-Arch mice (see methods) during induction. Light inactivation reduced SST-IN FR during TBS from 6.8 ± 1.2 Hz to 1.8 ± 0.4 Hz ($p<0.05$, WSR test, **Fig 2A2**). In PNs, SST-IN inactivation enhanced EPSP summation and depolarization during TBS (**Fig 2B1**). Inactivation of SST-INs during induction promotes robust LTP of L1b synapses **(Fig 2C1-3)**. EPSP amplitude was significantly enhanced post induction (in mV, Pre: 3.0 ± 0.3, Post: 4.7 ± 0.45, p: 0.007, n=16, paired t-test) and normalized EPSP amplitude and

area were significantly greater than 1 (Amplitude: 1.7 ± 0.2, p: 0.005; Area: 1.8 ± 0.2, p: 0.004, one sample t-test). Antagonism of NMDA receptors (DL-APV, 10 mM, **Fig 1B2**) in conjunction with light inactivation of SST-INs prevented LTP (**Fig C1, black circles, Supplemental Table 1**). These findings demonstrate that SST-IN inhibition regulates NMDA-dependent associative LTP at L1b intracortical synapses.

Inhibition of interneurons by VIP-INs

In other cortices, VIP interneurons inhibit SST-INs and PV-INs (Pfeffer, Xue et al. 2013, Pi, Hangya et al. 2013). Typically, VIP-cre mice are crossed with mice that express GFP in SST-INs (GIN-mice) or PV-INs (G42-mice). However, these lines sparsely label SST and PV-INs in APC (Large, Kunz et al. 2016). Instead, we used intrinsic properties for genetically identified interneuron classes in APC (Large, Kunz et al. 2016) to identify putative (p) SST-INs and pPV-INs in slices from VIP-ChR2 mice (**Supplemental Table 2**). Interneurons that could not be confidently identified were excluded from analysis. Neurons were recorded in three conditions: voltage clamp with Cs-Gluconate-Qx internal (IPSCs, +30 mV) or K-Gluconate-Qx internal (IPSCs, 0 mV) and current clamp with K-Gluconate (IPSPs at -50 mV). IPSC recordings were most reliable with Cs-Glu-Qx and the data presented are from this condition (**Figure 3)**. Data from remaining conditions are presented in **Supplemental Table 2**.

VIP-INs were activated by blue light pulses (5 ms) and IPSCs were recorded in postsynaptic neurons. VIP-INs inhibited nearly all recorded pSST-INs (86%), most pPV-INs (90%) and PNs (88%). High connectivity with SST and PV cells was expected (Pfeffer, Xue et al. 2013). However, unexpectedly high PN connections may reflect recording conditions as few connections were found with K-Glu-QX (27%) or K-Glu (0%) solutions. VIP-INs strongly inhibited pSST-INs (IPSC amplitude: 303 ± 57 pA, n=19) but weakly inhibited pPV-INs (35 ± 5.8 pA, n=9, p: 0.0008) and PNs (61 ± 14 pA, p: 0.001 n=14, ANOVA). To determine if VIP-IN inhibition can be sustained throughout TBS, light pulses (100 ms duration) were delivered at

theta frequency (10 pulses, **Fig 3A2**). We found that IPSC strength decreased by ~30% by the 5th pulse in all cell types then stabilized (SST: 31 ± 10%, p: 0.002; PV: 31± 5%, p: 0.06; PC: 28 ± 12%, p: 0.02, paired t-test, **Fig 3B2**).

Next, we depolarized pSST-INs to near-threshold membrane potentials (~-55 mV, K-Glu internal) and evoked strong IPSPs (2.02 ± 0.38 mV, n=18, **Fig 3C1**). We could not record IPSPs in PNs and PV neurons due to a combination of low input resistance and weak VIP-mediated IPSCs. With suprathreshold depolarization of pSST-INs we found that IPSPs deleted or delayed spikes by an average of 77 ± 26 ms (p: 0.016, n=11, paired t-test) compared to non-light trials (**Fig 3C1,3 left**). Finally, pSST-IN spike responses were diminished with theta activation of VIP-INs during TBS compared to non-light trials (OFF: 5.0 ± 0.6 Hz, ON: 3.5 ± 0.5, p: 0.002, n=11, paired t-test, **Fig 3C**).

Activation of VIP-INs promotes LTP

VIP-to-SST inhibition is a candidate circuit motif for dendritic disinhibition of PNs. However, without optogenetic activation, VIP-INs are only weakly driven by TBS (0.7 ± 0.6 Hz, n=6). This lack of VIP-IN recruitment is consistent with the inability to induce LTP under control conditions (**Fig 1B**). Light activation of VIP-INs enhanced FR during TBS (14 ± 4.0 Hz, p<0.05, WSR test **Fig 4A2**). Surprisingly, PN FR was unaffected by activation of VIP-INs during TBS (Light OFF: 6.2 ± 0.9 Hz, ON: 6.0 ± 1.1 Hz, n=7, p>0.05, WSR, **Fig 4B1)**. Nonetheless, activating VIP-INs enhanced EPSP summation in PNs during TBS **(Fig 4B2)**. Further, activation of VIP-INs during induction lead to robust LTP (**Fig 4C1**, EPSP amplitude in mV, Pre: 3.8 ± 0.8, Post: 5.1 ± 0.90, p: 0.002, n=10, paired t-test). Normalized amplitude and area were significantly >1 post induction (Amplitude: 1.5 ± 0.1, p: 0.003; Area: 1.7 ± 0.1, p: 0.0001, one sample t-test). Finally, LTP is blocked in the presence of the NMDAR antagonist, DL-APV (**Fig 4C1,**

Supplemental Table 1). These findings support a role for a VIP-SST-PN disinhibitory circuit in gating associative LTP at intracortical synapses.

Inactivation of PV-INs promotes LTP

Finally, we investigated whether optogenetic inactivation of PV-INs expressing Arch also promotes associative LTP (**Fig 5A1**). PV-INs are robustly activated during TBS **(Fig 5A2)** and light inactivation significantly decreased FR (Light OFF: 7.2 ± 2.5 Hz, ON: 2.8 ± 1.7 Hz, n=5, p<0.05, WSR, **Fig 5A2, right)**. In a number of PNs, this enhanced EPSP summation **(Fig 5B1**) and FR consistent with somatic disinhibition. PN FR appeared greater during PV inactivation (PV-Arch: 7.1 ± 1.7 Hz) versus manipulation of SST-INs or VIP-INs during TBS but this was not significant (SST-Arch: 5.7 ± 1.4 Hz; VIP-ChR2: 3.7 ± 1.2 Hz, p>0.05 ANOVA) **(Fig 5B2).** PV-IN inactivation during induction promoted LTP **(Fig 5C1-C3,** EPSP in mV, Pre: 2.0 ± 0.3, Post: 2.8 ± 0.4, p: 0.003, n=13, paired t-test). Normalized amplitude and area were significantly >1 post induction (Amplitude: 1.5 ± 0.1, p: 0.004; Area: 1.6 ± 0.1, p: 0.004, one sample t-test). LTP was blocked in the presence of the NMDAR antagonist, DL-APV (**Fig 5C1, Supplemental Table 1**). Since PV-INs primarily inhibit somas, PV-inactivation might promote LTP through action potential (AP) back-propagation into the dendrite (Johenning, Beed et al. 2009). To test this, we evoked APs in PNs during induction (5 Hz, ~1-2 APs per theta burst) without manipulating inhibition. This enhanced normalized EPSP amplitudes 25-30 min post pairing (1.4 ± 0.1, p: <-0.05, n=6, WSR, **Fig 5D1,2** gray triangles). Conversely, in a subset of PNs, LTP was not induced with inactivation of PV-INs resulting PN FRs that were <2 Hz (Norm. Amp: 1.0 ± 0.1, p:> 0.05, n=8, WSR, **Fig 5D1,2** open circles). To determine if APs are necessary, we investigated the subsets of PNs with low FR (<2 Hz) during SST-IN inactivation or VIP-IN activation. Despite low firing rates during induction, there was robust LTP in these PNs (Norm. Amplitude SST: 1.7 ± 0.3, p: <0.05, n=8; VIP: 1.6 ± 0.1, p: <0.05, n=7, WSR, **Fig 5D3**). This suggests that relief of dendritic inhibition through a VIP-to-SST-to-PN circuit is sufficient to

promote LTP without high FR. However, in the absence of dendritic disinhibition, LTP can be induced through backpropagation if PN firing rate is sufficiently high (>5 Hz). These two mechanisms could work in concert to promote ensemble formation in APC.

Discussion

It has been hypothesized that odor ensembles are formed through associative plasticity between co-activated pyramidal neurons (Haberly 2001, Wilson and Sullivan 2011). Intracortical synapses are stronger in animals that have learned an olfactory discrimination task (Saar, Grossman et al. 2002, Saar, Reuveni et al. 2012) and the induction of associative LTP *in vitro* is occluded in animals that have learned tasks (Lebel, Grossman et al. 2001). This capacity for enhancement as well as highly recurrent excitation (Poo and Isaacson 2011) necessitates strong inhibition to regulate neural activity (Luna and Schoppa 2008, Poo and Isaacson 2011, Bolding and Franks 2018) and synaptic plasticity (Kanter and Haberly 1993, Kanter, Kapur et al. 1996). Our present findings are consistent with a VIP->SST->PN circuit that transiently disinhibits PN dendrites to promote synaptic plasticity during odor learning while overall inhibition remains intact. This LTP does not depend on high post-synaptic spike rates, but backpropagation could contribute to synaptic enhancement.

Associative LTP at intracortical synapses within APC is well-characterized (Stripling, Patneau et al. 1988, Kanter and Haberly 1993, Poo and Isaacson 2007). Strong afferent excitation depolarizes apical PN dendrites and promotes NMDA receptor dependent potentiation of co-activated intracortical synapses. However, stimulation of both pathways also recruits strong inhibition and LTP is rarely induced in the absence of $GABA_AR$ antagonists (Kanter and Haberly 1993). We reproduced previous findings (Kanter, Kapur et al. 1996, Kumar, Schiff et al. 2018), and demonstrate that SST-IN mediated dendritic inhibition is blocked by dendritic application of Gabazine. We further demonstrate that a transient decrease in SST-IN activity at an opportune moment, i.e. during TBS, is sufficient to promote LTP. Thus, a circuit

mechanism that transiently inhibits SST-INs can gate synaptic plasticity. Throughout the cortex, VIP-INs inhibit SST-INs and potentially disinhibit PNs (Lee, Kruglikov et al. 2013, Pfeffer, Xue et al. 2013, Karnani, Jackson et al. 2016). Here, we show that VIP-INs strongly inhibit putative SST-INs, but weakly inhibit putative PV-INs as well as PNs. Further, optogenetic activation of VIP-INs decreases SST-IN spike responses during TBS and is sufficient gate associative LTP. These findings provide strong support that a VIP->SST->PN disinhibitory circuit gates intracortical synaptic plasticity in APC.

Our study complements a recent study in somatosensory cortex that used chemogenetics to inhibit VIP-INs or SST-INs and prevent or promote LTP induction respectively (Williams and Holtmaat 2019). Together, these two studies support a common VIP->SST->PN disinhibitory circuit motif regulates synaptic plasticity across cortical areas. However, pharmacological and chemogenetic methods of disinhibition could have long-term and/or non-specific effects on inhibition and network excitability. A benefit of optogenetics, is the ability to isolate the influence of disinhibition to the brief time window when afferent and intracortical pathways are co-activated. Thus, transient dendritic disinhibition is sufficient to gate the cascade of intracellular mechanisms underlying synaptic enhancement. Circuit mechanisms that provide well-timed input to VIP cells in conjunction with odor sampling could play a key role in odor learning and ensemble formation.

Interestingly, VIP-INs are not recruited by pairing afferent and intracortical stimulation, this may underlie the inability induce associative LTP with inhibition intact (**Fig 1**). At present, it is not known how VIP-INs in APC are recruited. In other cortices, VIP-IN activity is enhanced by arousal, locomotion, task engagement or reward (Lee, Kruglikov et al. 2013, Pi, Hangya et al. 2013, Fu, Tucciarone et al. 2014, Jackson, Ayzenshtat et al. 2016), either through additional excitatory drive from other cortical areas (Lee, Kruglikov et al. 2013, Williams and Holtmaat 2019) or through neuromodulation (Porter, Cauli et al. 1999, Lee, Hjerling-Leffler et al. 2010, Alitto and Dan 2012, Kuchibhotla, Gill et al. 2017, Pronneke, Witte et al. 2019). The APC

receives input from higher cortices including orbitofrontal cortex (Illig 2005) and neuromodulatory centers (Zaborszky, Carlsen et al. 1986, Linster, Wyble et al. 1999). Both of these pathways have been implicated in olfactory learning and plasticity (Patil, Linster et al. 1998, Patil and Hasselmo 1999, Linster, Maloney et al. 2003, Li, Luxenberg et al. 2006, Chapuis and Wilson 2013, Cohen, Wilson et al. 2015, Strauch and Manahan-Vaughan 2018). Future studies are needed to ascertain the potential links between descending excitation and/or neuromodulation, the recruitment of VIP-INs, and the gating of synaptic plasticity during olfactory processing.

Finally, an unexpected finding was that PN firing rates do not change when VIP-INs are activated during LTP induction. Likewise, inactivation of SST-INs minimally influenced PN firing rates but promoted LTP. Inhibition from SST-INs typically suppresses PN firing rates in APC (Sturgill and Isaacson 2015). Conversely, disinhibition through a VIP-SST-PN circuit would be expected to enhance PN firing rates (Pi, Hangya et al. 2013, Fu, Tucciarone et al. 2014, Karnani, Jackson et al. 2016). Our findings suggest that VIP-SST-PN disinhibition can impact ensemble responses at a subthreshold level in the dendrites. Conversely, inactivation of PV-INs also promotes LTP but requires higher PN firing rates during LTP induction. Artificially increasing postsynaptic firing rates during TBS promotes LTP through spike backpropagation (Bathellier, Margrie et al. 2009). It is conceivable that VIP-INs also gate plasticity through a VIP-PV-PN circuit. However, we predict this circuit motif contributes minimally to LTP induction for two reasons. First, VIP-INs weakly inhibit PV-INs. And second, SST-INs strongly inhibit PV-INs in APC and other cortices (Pfeffer, Xue et al. 2013, Xu, Jeong et al. 2013, Large, Kunz et al. 2016). Driving VIP-INs and inhibiting SST-INs, likely increases PV-IN activity and somatic inhibition resulting in minimal changes in PN firing rates. Altogether, we show that LTP can be induced at intracortical synapses through spike dependent and independent pathways mediated through PV-INs and SST-INs respectively.

Though many previous studies have focused on the influence of disinhibitory circuits on FR or behavior, our study highlights a role for disinhibition in the subthreshold dynamics that gate long-term plasticity. We have elucidated two potential circuit mechanisms to promote intracortical synaptic plasticity and the formation of olfactory representations. Specifically, our findings suggest that the VIP-SST-PN circuit motif plays a central role in gating synaptic plasticity in PN dendrites. However, additional circuit mechanisms that regulate PV-IN activity could secondarily gate LTP through suprathreshold mechanisms. These findings demonstrate the challenge of the delineating roles for the individual circuit motifs that are nested in complex neural networks. It remains to be determined if these mechanisms work in concert, or at different stages of afferent and recurrent olfactory processing.

Figure 1: Associative LTP of intracortical synapses is gated by dendritic disinhibition. **A)** Schematic of APC circuit and stimulation paradigm. Strong (s) TBS of afferents (L1a) is paired with weak (w) single-pulses at the intracortical pathway (L1b). **B)** Normalized EPSP amplitude pre (-5 to 0 min) and post induction (gray box) with inhibition intact (black) or with dendritic application of Gabazine (GZ, brown). **C)** Inhibition intact: L1b average EPSP amplitude 25-30 min post induction (black circles) compared to baseline (Pre, open circles). Right: Normalized EPSP amplitude, area and input resistance (R_{in}). **D1)** Schematic of GZ at PN dendrites. **D2)** Left: L1b EPSP pre (black) and post (brown) induction with GZ. Right: L1b EPSP amplitude post (brown circles) versus baseline (open circles). **D3)** Normalized EPSP area is significantly greater than 1 (*p: 0.047). Amplitude is significantly>1 in absence of outlier (red circle, ** p: 0.005). **E)** GZ blocks optically evoked IPSPs (reversed at -85 mV) from SST-ChR2 mice. Left: IPSPs prior to GZ application (black), at baseline (magenta) and post pairing (pink, time points indicated by arrows in Fig 1B). Right: IPSPs were significantly diminished (**p: 0.002) by GZ application to a stable baseline (pre, magenta) that remained post pairing (post, pink).

Figure 2: SST-interneuron inactivation promotes associative LTP. A1) Schematic: SST-INs express Archaerhodopsin (Arch). **A2)** SST-IN responses during TBS in control (black) and inactivated (green) conditions (*p<0.05, WSR test). **B)** PN responses for a single TBS burst. **Left :** Inactivation of SST-INs enhanced PN depolarization (green vs. black trace). **Right:** Depolarization during SST-IN inactivation (green) is reduced by APV (gray trace). **C1)** Normalized EPSP amplitude following pairing with SST-IN inactivation (magenta circles). LTP is blocked by APV (black). **C2)** EPSP amplitudes were enhanced post pairing (magenta trace, filled circles) compared to baseline (black trace, open circles, **p: 0.007, paired t-test). **C3)** Normalized EPSP amplitude (**p: 0.005) and area (**p: 0.004, one sample t-test) were >1 post pairing.

Figure 3: Inhibition by VIP-interneurons in piriform cortex. A1) VIP-INs express ChR2. Optically evoked IPSCs were recorded in putative(p) pSST-INs (magenta), pPV-INs (blue) and PNs (black). **A2)** Responses of the same neurons (A1) to ten light pulses (100 ms duration, 4 Hz). **B1)** IPSC amplitude was stronger in pSST-INs versus pPV-INs (*p:0.014) or PNs (*p:0.042, ANOVA). **B2**) In pSST-INs, IPSC amplitude diminishes by the 5th pulse of theta stimulation (**p: 0.009, paired t-test). **C1)** IPSCs from VIP-INs delay pSST-IN spike responses during suprathreshold depolarization (4 overlaid traces) **Left:** Control, **Right**: activation of VIP-INs (100 ms pulse, blue). Magenta trace: VIP-IN mediated IPSC during subthreshold depolarization. **C2)** Interspike interval (ISI) was significantly increased during optical activation of VIP-INs (blue circles, p: 0.016, paired t-test, n=11) compared to light off trials (black circles). **D1)** Spike responses in pSST-INs during TBS in control (magenta trace) and during pulsed light (blue trace). **D2**) pSST-IN firing rates decreased during TBS on light trials (blue) versus control (black circles, p:0.002, paired t-test, n=11).

Figure 4: VIP-interneuron activation promotes associative LTP. A1) Circuit schematic: VIP-INs express ChR2 and were activated using theta pulsed light during L1a+L1b pairing. **A2)** VIP-IN responses during TBS without (black) and with light (blue). FRs increase during pairing with light (blue circles, $p<0.05$, WSR, n=7). **B1)** VIP-IN activation did not increase PN FR during pairing ($p>0.05$, WSR, n=5). **B2)** Top: Activation of VIP-INs enhanced PN depolarization during TBS stimulation (blue vs. black trace). Bottom: PN depolarization during VIP-IN activation (blue trace) is reduced by APV (gray trace). **C1)** Normalized EPSP amplitude pre and post pairing with VIP-IN activation (green circles). LTP is blocked by APV (black). **C2)** EPSP amplitudes were enhanced 25 min post pairing (green trace, filled circles) compared to baseline (black trace, open circles, **p: 0.002, paired t-test). **C3)** Normalized EPSP amplitude (**p: 0.003) and area (**p: 0.0001, one sample t-test) were >1 post pairing.

Figure 5: PV-interneuron inactivation during induction promotes associative LTP. A1) Schematic of inactivation of PV-Arch interneurons during induction. **A2)** Decreased PV-IN spiking during inactivation (green) compared to control (black, *p<0.05, WSR, n=5). **B1)** PV-IN inactivation enhanced PN depolarization during TBS (green vs. black trace). **B2)** PN firing rates during induction with PV-IN (blue) or SST-IN (magenta) inactivation or VIP-IN activation (green). **C1)** Normalized EPSP amplitude with PV-IN inactivation (blue) or inactivation plus APV (black). **C2)** Enhancement of EPSP amplitude 25-30 min post induction (blue trace, filled circles) compared to baseline (black trace, open circles, **p: 0.003, paired t-test). **C3)** Normalized EPSP amplitude (**p: 0.004) and area (**p: 0.004, 1 sample t-test) were >1. **D1**) Normalized EPSP amplitude in two conditions- 1) inhibition intact and evoked backpropagating APs in the PN during induction (FR>5 Hz, gray triangles, n=6) and 2) PV-IN inactivation and PN FR <2 Hz during induction (open blue circles, n=8). **D2)** Normalized EPSP amplitude 25-30 min post induction with PV-IN inactivation for low PN FR (<2Hz, open circles), high PN FR (>5Hz, solid circles,* p: <0.05, WSR) or evoked backpropagation (BP>5Hz, gray triangles,* p: <0.05, WSR). **D3)** Normalized EPSP amplitude 25-30 min post induction (left axis) conditioned on <2 Hz FR in PNs (right axis, squares). Shown for PV-IN inactivation (open blue circles), SST-IN inactivation, (solid magenta, * p: <0.05, WSR) or VIP-IN activation (green circles,* p: <0.05, WSR). Average firing rate for each group is also shown (right axis, mean +/- SE, squares).

References

Abbott, L. F. and S. B. Nelson (2000). "Synaptic plasticity: taming the beast." Nat Neurosci **3 Suppl**: 1178-1183.

Alitto, H. J. and Y. Dan (2012). "Cell-type-specific modulation of neocortical activity by basal forebrain input." Front Syst Neurosci **6**: 79.

Artinian, J. and J. C. Lacaille (2018). "Disinhibition in learning and memory circuits: New vistas for somatostatin interneurons and long-term synaptic plasticity." Brain Res Bull **141**: 20-26.

Bathellier, B., T. W. Margrie and M. E. Larkum (2009). "Properties of piriform cortex pyramidal cell dendrites: implications for olfactory circuit design." J Neurosci **29**(40): 12641-12652.

Bolding, K. A. and K. M. Franks (2018). "Recurrent cortical circuits implement concentration-invariant odor coding." Science **361**(6407).

Carey, R. M. and M. Wachowiak (2011). "Effect of sniffing on the temporal structure of mitral/tufted cell output from the olfactory bulb." J Neurosci **31**(29): 10615-10626.

Chapuis, J. and D. A. Wilson (2013). "Cholinergic modulation of olfactory pattern separation." Neurosci Lett **545**: 50-53.

Cohen, Y., D. A. Wilson and E. Barkai (2015). "Differential modifications of synaptic weights during odor rule learning: dynamics of interaction between the piriform cortex with lower and higher brain areas." Cereb Cortex **25**(1): 180-191.

Franks, K. M., M. J. Russo, D. L. Sosulski, A. A. Mulligan, S. A. Siegelbaum and R. Axel (2011). "Recurrent circuitry dynamically shapes the activation of piriform cortex." Neuron **72**(1): 49-56.

Fu, Y., J. M. Tucciarone, J. S. Espinosa, N. Sheng, D. P. Darcy, R. A. Nicoll, Z. J. Huang and M. P. Stryker (2014). "A cortical circuit for gain control by behavioral state." Cell **156**(6): 1139-1152.

Haberly, L. B. (2001). "Parallel-distributed processing in olfactory cortex: new insights from morphological and physiological analysis of neuronal circuitry." Chem Senses **26**(5): 551-576.

Haberly, L. B. and J. L. Price (1977). "The axonal projection patterns of the mitral and tufted cells of the olfactory bulb in the rat." Brain Res **129**(1): 152-157.

Haberly, L. B. and J. L. Price (1978). "Association and commissural fiber systems of the olfactory cortex of the rat. II. Systems originating in the olfactory peduncle." J Comp Neurol **181**(4): 781-807.

Igarashi, K. M., N. Ieki, M. An, Y. Yamaguchi, S. Nagayama, K. Kobayakawa, R. Kobayakawa, M. Tanifuji, H. Sakano, W. R. Chen and K. Mori (2012). "Parallel mitral and tufted cell pathways route distinct odor information to different targets in the olfactory cortex." J Neurosci **32**(23): 7970-7985.

Illig, K. R. (2005). "Projections from orbitofrontal cortex to anterior piriform cortex in the rat suggest a role in olfactory information processing." J Comp Neurol **488**(2): 224-231.

Illig, K. R. and L. B. Haberly (2003). "Odor-evoked activity is spatially distributed in piriform cortex." J Comp Neurol **457**(4): 361-373.

Jackson, J., I. Ayzenshtat, M. M. Karnani and R. Yuste (2016). "VIP+ interneurons control neocortical activity across brain states." J Neurophysiol **115**(6): 3008-3017.

Johenning, F. W., P. S. Beed, T. Trimbuch, M. H. Bendels, J. Winterer and D. Schmitz (2009). "Dendritic compartment and neuronal output mode determine pathway-specific long-term potentiation in the piriform cortex." The Journal of Neuroscience **29**(43): 13649-13661.

Kanter, E. D. and L. B. Haberly (1993). "Associative long-term potentiation in piriform cortex slices requires GABAA blockade." J Neurosci **13**(6): 2477-2482.

Kanter, E. D., A. Kapur and L. B. Haberly (1996). "A dendritic GABAA-mediated IPSP regulates facilitation of NMDA-mediated responses to burst stimulation of afferent fibers in piriform cortex." J Neurosci **16**(1): 307-312.

Karnani, M. M., J. Jackson, I. Ayzenshtat, A. Hamzehei Sichani, K. Manoocheri, S. Kim and R. Yuste (2016). "Opening Holes in the Blanket of Inhibition: Localized Lateral Disinhibition by VIP Interneurons." J Neurosci **36**(12): 3471-3480.

Kepecs, A., N. Uchida and Z. F. Mainen (2007). "Rapid and precise control of sniffing during olfactory discrimination in rats." J Neurophysiol **98**(1): 205-213.

Kuchibhotla, K. V., J. V. Gill, G. W. Lindsay, E. S. Papadoyannis, R. E. Field, T. A. Sten, K. D. Miller and R. C. Froemke (2017). "Parallel processing by cortical inhibition enables context-dependent behavior." Nat Neurosci **20**(1): 62-71.

Kumar, A., O. Schiff, E. Barkai, B. W. Mel, A. Poleg-Polsky and J. Schiller (2018). "NMDA spikes mediate amplification of inputs in the rat piriform cortex." Elife **7**.

Large, A. M., N. A. Kunz, S. L. Mielo and A. M. Oswald (2016). "Inhibition by Somatostatin Interneurons in Olfactory Cortex." Front Neural Circuits **10**: 62.

Large, A. M., N. W. Vogler, S. Mielo and A. M. Oswald (2016). "Balanced feedforward inhibition and dominant recurrent inhibition in olfactory cortex." Proc Natl Acad Sci U S A **113**(8): 2276-2281.

Lebel, D., Y. Grossman and E. Barkai (2001). "Olfactory learning modifies predisposition for long-term potentiation and long-term depression induction in the rat piriform (olfactory) cortex." Cereb Cortex **11**(6): 485-489.

Lee, S., J. Hjerling-Leffler, E. Zagha, G. Fishell and B. Rudy (2010). "The largest group of superficial neocortical GABAergic interneurons expresses ionotropic serotonin receptors." The Journal of Neuroscience **30**(50): 16796-16808.

Lee, S., I. Kruglikov, Z. J. Huang, G. Fishell and B. Rudy (2013). "A disinhibitory circuit mediates motor integration in the somatosensory cortex." Nat Neurosci **16**(11): 1662-1670.

Li, W., E. Luxenberg, T. Parrish and J. A. Gottfried (2006). "Learning to smell the roses: experience-dependent neural plasticity in human piriform and orbitofrontal cortices." Neuron **52**(6): 1097-1108.

Linster, C., M. Maloney, M. Patil and M. E. Hasselmo (2003). "Enhanced cholinergic suppression of previously strengthened synapses enables the formation of self-organized representations in olfactory cortex." Neurobiol Learn Mem **80**(3): 302-314.

Linster, C., B. P. Wyble and M. E. Hasselmo (1999). "Electrical stimulation of the horizontal limb of the diagonal band of broca modulates population EPSPs in piriform cortex." J Neurophysiol **81**(6): 2737-2742.

Lucas, E. K. and R. L. Clem (2018). "GABAergic interneurons: The orchestra or the conductor in fear learning and memory?" Brain Res Bull **141**: 13-19.

Luna, V. M. and N. E. Schoppa (2008). "GABAergic circuits control input-spike coupling in the piriform cortex." J Neurosci **28**(35): 8851-8859.

Madisen, L., T. Mao, H. Koch, J. M. Zhuo, A. Berenyi, S. Fujisawa, Y. W. Hsu, A. J. Garcia, 3rd, X. Gu, S. Zanella, J. Kidney, H. Gu, Y. Mao, B. M. Hooks, E. S. Boyden, G. Buzsaki, J. M. Ramirez, A.

R. Jones, K. Svoboda, X. Han, E. E. Turner and H. Zeng (2012). "A toolbox of Cre-dependent optogenetic transgenic mice for light-induced activation and silencing." Nat Neurosci **15**(5): 793-802.

Malenka, R. C. and M. F. Bear (2004). "LTP and LTD: an embarrassment of riches." Neuron **44**(1): 5-21.

Mombaerts, P., F. Wang, C. Dulac, S. K. Chao, A. Nemes, M. Mendelsohn, J. Edmondson and R. Axel (1996). "Visualizing an olfactory sensory map." Cell **87**(4): 675-686.

Patil, M. M. and M. E. Hasselmo (1999). "Modulation of inhibitory synaptic potentials in the piriform cortex." J Neurophysiol **81**(5): 2103-2118.

Patil, M. M., C. Linster, E. Lubenov and M. E. Hasselmo (1998). "Cholinergic agonist carbachol enables associative long-term potentiation in piriform cortex slices." J Neurophysiol **80**(5): 2467-2474.

Pfeffer, C. K., M. Xue, M. He, Z. J. Huang and M. Scanziani (2013). "Inhibition of inhibition in visual cortex: the logic of connections between molecularly distinct interneurons." Nat Neurosci **16**(8): 1068-1076.

Pi, H. J., B. Hangya, D. Kvitsiani, J. I. Sanders, Z. J. Huang and A. Kepecs (2013). "Cortical interneurons that specialize in disinhibitory control." Nature **503**(7477): 521-524.

Poo, C. and J. S. Isaacson (2007). "An early critical period for long-term plasticity and structural modification of sensory synapses in olfactory cortex." J Neurosci **27**(28): 7553-7558.

Poo, C. and J. S. Isaacson (2009). "Odor representations in olfactory cortex: "sparse" coding, global inhibition, and oscillations." Neuron **62**(6): 850-861.

Poo, C. and J. S. Isaacson (2011). "A major role for intracortical circuits in the strength and tuning of odor-evoked excitation in olfactory cortex." Neuron **72**(1): 41-48.

Porter, J. T., B. Cauli, K. Tsuzuki, B. Lambolez, J. Rossier and E. Audinat (1999). "Selective excitation of subtypes of neocortical interneurons by nicotinic receptors." The Journal of Neuroscience **19**(13): 5228-5235.

Pronneke, A., M. Witte, M. Mock and J. F. Staiger (2019). "Neuromodulation Leads to a Burst-Tonic Switch in a Subset of VIP Neurons in Mouse Primary Somatosensory (Barrel) Cortex." Cereb Cortex.

558 Rennaker, R. L., C. F. Chen, A. M. Ruyle, A. M. Sloan and D. A. Wilson (2007). "Spatial and
559 temporal distribution of odorant-evoked activity in the piriform cortex." J Neurosci **27**(7):
560 1534-1542.
561 Saar, D., Y. Grossman and E. Barkai (2002). "Learning-induced enhancement of
562 postsynaptic potentials in pyramidal neurons." J Neurophysiol **87**(5): 2358-2363.
563 Saar, D., I. Reuveni and E. Barkai (2012). "Mechanisms underlying rule learning-induced
564 enhancement of excitatory and inhibitory synaptic transmission." J Neurophysiol **107**(4):
565 1222-1229.
566 Sosulski, D. L., M. L. Bloom, T. Cutforth, R. Axel and S. R. Datta (2011). "Distinct
567 representations of olfactory information in different cortical centres." Nature **472**(7342):
568 213-216.
569 Stettler, D. D. and R. Axel (2009). "Representations of odor in the piriform cortex." Neuron
570 **63**(6): 854-864.
571 Stokes, C. C. and J. S. Isaacson (2010). "From dendrite to soma: dynamic routing of
572 inhibition by complementary interneuron microcircuits in olfactory cortex." Neuron **67**(3):
573 452-465.
574 Strauch, C. and D. Manahan-Vaughan (2018). "In the Piriform Cortex, the Primary Impetus
575 for Information Encoding through Synaptic Plasticity Is Provided by Descending Rather
576 than Ascending Olfactory Inputs." Cereb Cortex **28**(2): 764-776.
577 Stripling, J. S., D. K. Patneau and C. A. Gramlich (1988). "Selective long-term potentiation in
578 the pyriform cortex." Brain Res **441**(1-2): 281-291.
579 Sturgill, J. F. and J. S. Isaacson (2015). "Somatostatin cells regulate sensory response fidelity
580 via subtractive inhibition in olfactory cortex." Nat Neurosci **18**(4): 531-535.
581 Suzuki, N. and J. M. Bekkers (2010a). "Distinctive classes of GABAergic interneurons
582 provide layer-specific phasic inhibition in the anterior piriform cortex." Cereb Cortex
583 **20**(12): 2971-2984.
584 Suzuki, N. and J. M. Bekkers (2010b). "Inhibitory neurons in the anterior piriform cortex of
585 the mouse: classification using molecular markers." J Comp Neurol **518**(10): 1670-1687.
586 Taniguchi, H., M. He, P. Wu, S. Kim, R. Paik, K. Sugino, D. Kvitsiani, Y. Fu, J. Lu, Y. Lin, G.
587 Miyoshi, Y. Shima, G. Fishell, S. B. Nelson and Z. J. Huang (2011). "A resource of Cre driver

588 lines for genetic targeting of GABAergic neurons in cerebral cortex." Neuron **71**(6): 995-
589 1013.
590 Williams, L. E. and A. Holtmaat (2019). "Higher-Order Thalamocortical Inputs Gate Synaptic
591 Long-Term Potentiation via Disinhibition." Neuron **101**(1): 91-102 e104.
592 Wilson, D. A. and R. M. Sullivan (2011). "Cortical processing of odor objects." Neuron **72**(4):
593 506-519.
594 Xu, H., H. Y. Jeong, R. Tremblay and B. Rudy (2013). "Neocortical somatostatin-expressing
595 GABAergic interneurons disinhibit the thalamorecipient layer 4." Neuron **77**(1): 155-167.
596 Zaborszky, L., J. Carlsen, H. R. Brashear and L. Heimer (1986). "Cholinergic and GABAergic
597 afferents to the olfactory bulb in the rat with special emphasis on the projection neurons in
598 the nucleus of the horizontal limb of the diagonal band." J Comp Neurol **243**(4): 488-509.
599

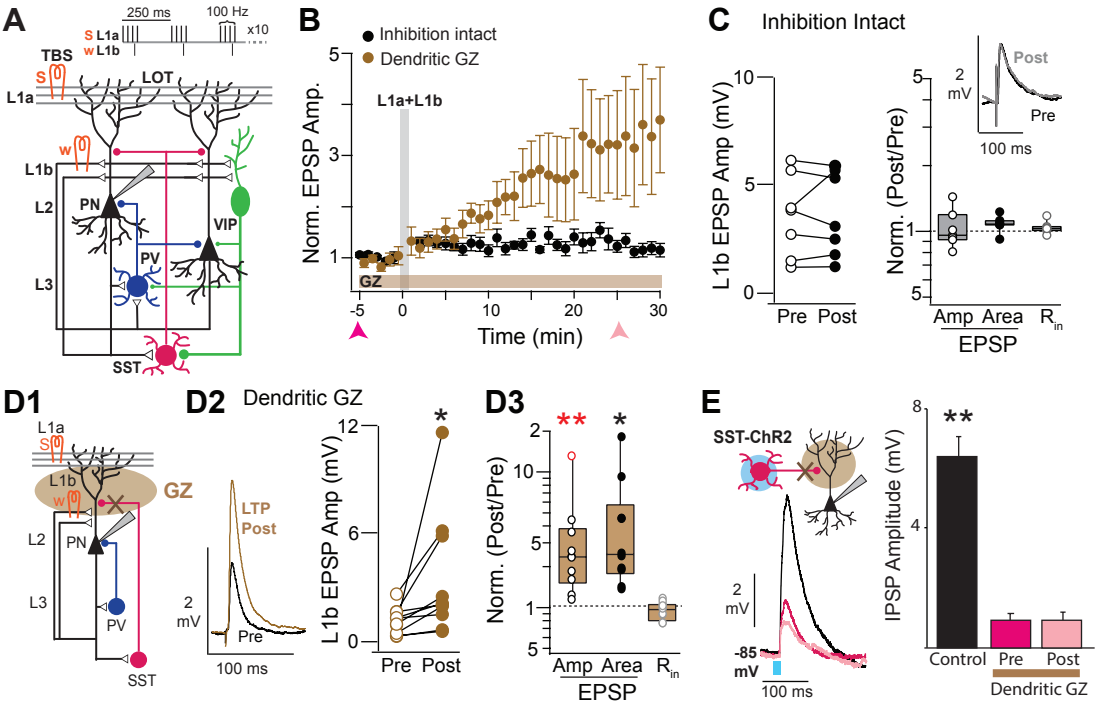

Figure 1: Associative LTP of intracortical synapses is gated by dendritic disinhibition.
A) Schematic of APC circuit and stimulation paradigm. Strong (s) TBS of afferents (L1a) is paired with weak (w) single-pulses at the intracortical pathway (L1b). B) Normalized EPSP amplitude pre (-5 to 0 min) and post induction (gray box) with inhibition intact (black) or with dendritic application of Gabazine (GZ, brown). C) Inhibition intact: L1b average EPSP amplitude 25-30 min post induction (black circles) compared to baseline (Pre, open circles). Right: Normalized EPSP amplitude, area and input resistance (Rin). D1) Schematic of GZ at PN dendrites. D2) Left: L1b EPSP pre (black) and post (brown) induction with GZ. Right: L1b EPSP amplitude post (brown circles) versus baseline (open circles). D3) Normalized EPSP area is significantly greater than 1 (*p: 0.047). Amplitude is significantly>1 in absence of outlier (red circle, ** p: 0.005). E) GZ blocks optically evoked IPSPs (reversed at -85 mV) from SST-ChR2 mice. Left: IPSPs prior to GZ application (black), at baseline (magenta) and post pairing (pink, time points indicated by arrows in Fig 1B). Right: IPSPs were significantly diminished (**p: 0.002) by GZ application to a stable baseline (pre, magenta) that remained post pairing (post, pink).

		PSP Amplitude (mV)			Norm. PSP Amplitude		Norm. PSP Area	
Condition	**# cells,mice**	**Pre (5 min)**	**Post (25-30 min)**	**p^1, Power**	**Amp (25-30 min)**	**p^2, Power**	**Area (25-30 min)**	**p^2, Power**
Control	**12, 5**	2.8 ± 0.5	2.9 ± 0.5	0.671	1.0 ± 0.1	0.48	1.2 ± 0.1	0.09
Dendritic GZ	**10, 8**	**1.1 ± 0.2**	**3.5 ± 1.1**	**0.048, <60%**	3.4 ± 1.1	0.058, 60%,	**4.8 ± 1.7**	**0.047, 60%**
Dendritic GZ-OL	**9, 8**	**1.2 ± 0.3**	**2.6 ± 0.7**	**0.020, 70%**	**2.5 ± 0.3**	**0.005**	**3.3 ± 0.8**	**0.027**
SST-Arch	**17,8**	**3.0 ± 0.3**	**4.7 ± 0.5**	**0.007**	**1.7 ± 0.2**	**0.005**	**1.8 ± 0.2**	**0.004**
SST-Arch < 2Hz	**8, 4**	**2.7 ± 0.4**	**4.2 ± 0.8**	**<0.05, 60%**	**1.7 ± 0.3**	**<0.05, 66%**	1.9 ± 0.4	>0.05, 64%
SST-Arch APV	**8, 4**	4.7 ± 0.9	3.9 ± 0.8	0.546	0.9 ± 0.1	>0.05	0.8 ± 0.1	0.16
VIP-ChR2	**10, 5**	**3.8 ± 0.8**	**5.1 ± 0.9**	**0.002**	**1.5 ± 0.1**	**0.003**	**1.7 ± 0.1**	**0.0001**
VIP-ChR2 <2Hz	**7, 3**	**2.6 ± 0.5**	**3.9 ± 0.6**	**<0.05**	**1.6 ± 0.1**	**<0.05**	**1.8 ± 0.1**	**<0.05**
VIP-ChR2 APV	**7, 3**	5.3 ± 1.4	5.3 ± 1.3	>0.05	1.0 ± 0.1	>0.05	1.0 ± 0.1	>0.05
PV-Arch	**13, 5**	**2.0 ± 0.3**	**2.8 ± 0.4**	**0.003**	**1.5 ± 0.1**	**0.004**	**1.6 ± 0.1**	**0.004**
PV-Arch-APV	**8, 3**	3.0 ± 0.4	2.9 ± 0.4	>0.05	1.0 ± 0.1	>0.05	1.0 ± 0.1	>0.05
PV-Arch <2 Hz	**8, 4**	1.9 ± 0.4	1.9 ± 0.4	>0.05	1.0 ± 0.1	>0.05	1.0 ± 0.1	>0.05
Backpropagation	**6, 3**	**4.0 ± 0.4**	**5.6 ± 1.0**	**<0.05, <60%**	**1.4 ± 0.1**	**<0.05**	**1.5 ± 0.2**	**<0.05, 72%**

Supplemental Table 1: Synaptic properties following Induction in various conditions Abbreviations: Amp, Amplitude; GZ, Gabazine; SST, Somatostatin; Arch, Archaerhodopsin; APV: DL-2-Amino-5-phosphonopentanoic acid; VIP: Vasoactive intestinal polypeptide; PV, Parvalbumin; Norm., Normalized to baseline. p^1 P-value, paired t-test or Wilcoxon Signed Rank(WSR) test if n<10; p^2 P-value single distribution t-test, or WSR for n<10. All results have power >80% at a 5% significance level except where lower power is indicated. Power was calculated based in number of cells for parametric tests and may be underestimated for non-parametric tests. For WSR, P-values are cannot be accurately calculated for n<10, only >/< 0.05 is given. There was one outlier with application of Dendritic GZ, statistics are presented with (GZ) and without the outlier (GZ-OL).

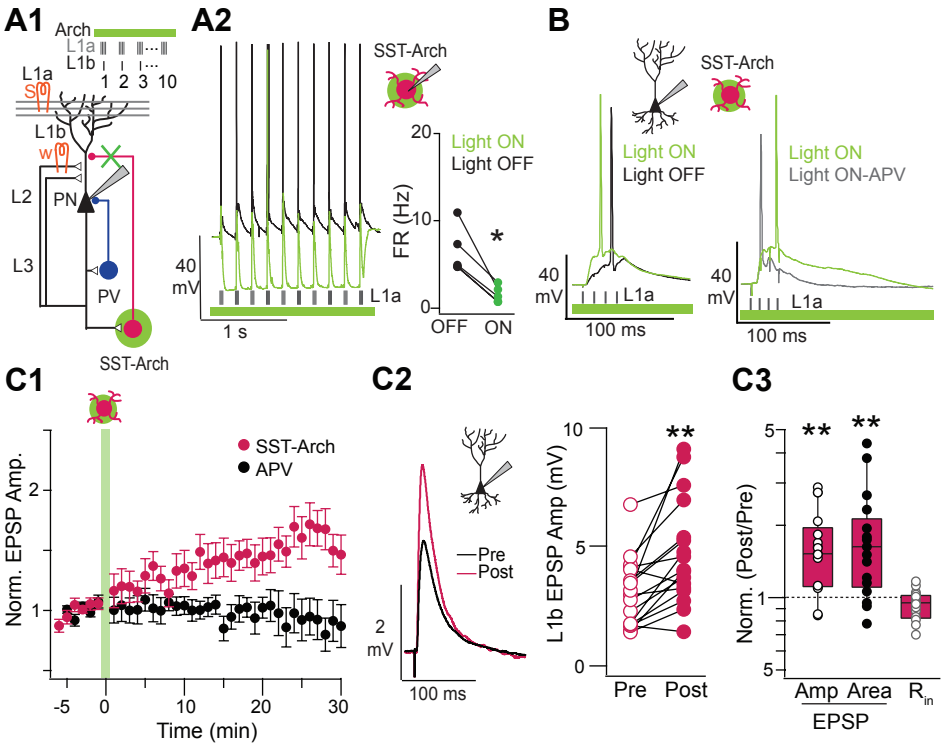

Figure 2: SST-interneuron inactivation promotes associative LTP. A1) Schematic: SST-INs express Archaerhodopsin (Arch). A2) SST-IN responses during TBS in control (black) and inactivated (green) conditions (*p<0.05, WSR test). B) PN responses for a single TBS burst. Left : Inactivation of SST-INs enhanced PN depolarization (green vs. black trace). Right: Depolarization during SST-IN inactivation (green) is reduced by APV (gray trace). C1) Normalized EPSP amplitude following pairing with SST-IN inactivation (magenta circles). LTP is blocked by APV (black). C2) EPSP amplitudes were enhanced post pairing (magenta trace, filled circles) compared to baseline (black trace, open circles, **p: 0.007, paired t-test). C3) Normalized EPSP amplitude (**p: 0.005) and area (**p: 0.004, one sample t-test) were >1 post pairing.

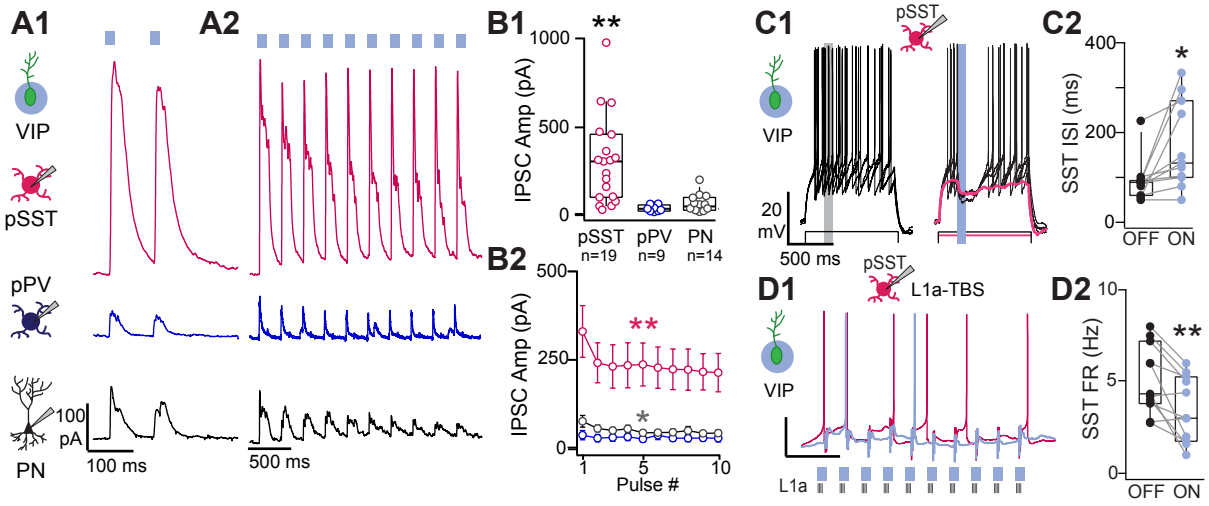

Figure 3: Inhibition by VIP-interneurons in piriform cortex. A1) VIP-INs express ChR2. Optically evoked IPSCs were recorded in putative(p) pSST-INs (magenta), pPV-INs (blue) and PNs (black). A2) Responses of the same neurons (A1) to ten light pulses (100 ms duration, 4 Hz). B1) IPSC amplitude was stronger in pSST-INs versus pPV-INs (*p:0.014) or PNs (*p:0.042, ANOVA). B2) In pSST-INs, IPSC amplitude diminishes by the 5th pulse of theta stimulation (**p: 0.009, paired t-test). C1) IPSCs from VIP-INs delay pSST-IN spike responses during suprathreshold depolarization (4 overlaid traces) Left: Control, Right: activation of VIP-INs (100 ms pulse, blue). Magenta trace: VIP-IN mediated IPSC during subthreshold depolarization. C2) Interspike interval (ISI) was significantly increased during optical activation of VIP-INs (blue circles, p: 0.016, paired t-test, n=11) compared to light off trials (black circles). D1) Spike responses in pSST-INs during TBS in control (magenta trace) and during pulsed light (blue trace). D2) pSST-IN firing rates decreased during TBS on light trials (blue) versus control (black circles, p:0.002, paired t-test, n=11).

		Intrinsic Properties			Synaptic Connectivity				
	Condition	R_{in} (MΩ)	Tau (ms)	Sag (mV)	# recorded	# connections	% VIP input	IPSC Amp (pA)	IPSC Amp (mV)
pSST-G1	**Criterion**	**>200**	**>10**	**>0.75**					
	Cs-Glu-Qx	255 ± 29	27 ± 1.7	1.4 ± 0.23	11	10	91	190 ± 45	
	K-Glu-Qx	222 ± 9.2	24 ± 2.2	1.2 ± 0.23	16	11	69	39 ± 10	
	K-Glu	312 ± 29	23 ± 1.9	2.0 ± 0.38	19	12	63		2.5 ± 0.5
pSST-G2	**Criterion**	**100-200**	**5-20**	**0.3-0.75**					
	Cs-Glu-Qx	135 ± 13	17 ± 2.0	0.67 ± 0.15	11	9	82	429 ± 96	
	K-Glu-Qx	143 ± 11	10 ± 0.9	0.36 ± 0.05	10	8	80	58 ± 16	
	K-Glu	110 ± 16	13 ± 1.2	0.24 ± 0.03	12	6	50		1.1 ± 0.3
pPV	**Criterion**	**50-150**	**<10**	**<0.3**					
	Cs-Glu-Qx	106 ± 12	7.8 ± 0.7	0.1 ± 0.02	10	9	90	35 ± 5.8	
	K-Glu-Qx	63 ± 3.0	6.7 ± 0.4	0.24 ± 0.03	15	11	73	31 ± 7.6	
PN	**Criterion**	**<200**	**<25**	**n/a**					
	Cs-Glu-Qx	105 ± 5.2	16 ± 0.8	0.25 ± 0.06	16	14	88	61 ± 14	
	K-Glu-Qx	130 ± 11	13 ± 1.3	0.32 ± 0.05	15	4	27	21 ± 7	
	K-Glu	123 ± 18	17 ± 1.4	0.45 ± 0.07	7	0	0		0

Supplemental Table 2: Inhibition mediated by VIP-Interneurons. Abbreviations: R_{in} , Input resistance; tau, membrane time constant; Sag, sag current; Glu, gluconate; QX, QX-314 sodium channel blocker. G1-group one type SST interneurons Martinotti, low threshold spiking; G2-group 2 SST interneurons, X98 or X94 like.

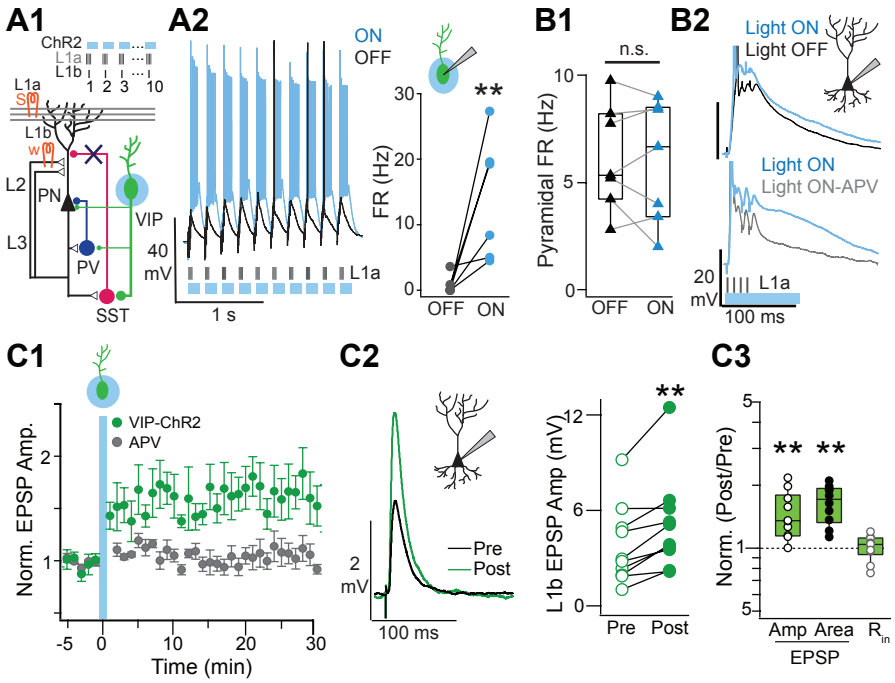

Figure 4: VIP-interneuron activation promotes associative LTP. A1) Circuit schematic: VIP-INs express ChR2 and were activated using theta pulsed light during L1a+L1b pairing. A2) VIP-IN responses during TBS without (black) and with light (blue). FRs increase during pairing with light (blue circles, $p<0.05$, WSR, n=7). B1) VIP-IN activation did not increase PN FR during pairing ($p>0.05$, WSR, n=5). B2) Top: Activation of VIP-INs enhanced PN depolarization during TBS stimulation (blue vs. black trace). Bottom: PN depolarization during VIP-IN activation (blue trace) is reduced by APV (gray trace). C1) Normalized EPSP amplitude pre and post pairing with VIP-IN activation (green circles). LTP is blocked by APV (black). C2) EPSP amplitudes were enhanced 25 min post pairing (green trace, filled circles) compared to baseline (black trace, open circles, **p: 0.002, paired t-test). C3) Normalized EPSP amplitude (**p: 0.003) and area (**p: 0.0001, one sample t-test) were >1 post pairing.

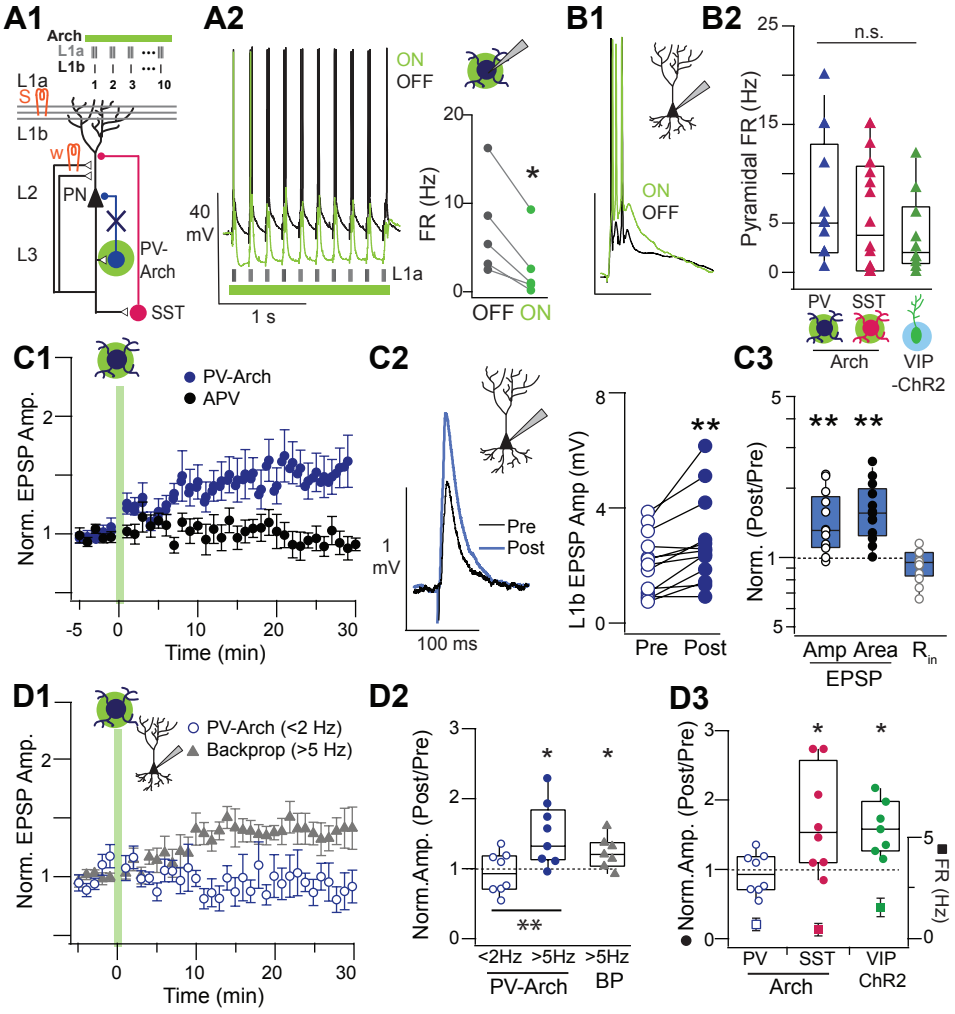

Figure 5: PV-interneuron inactivation during induction promotes associative LTP. A1) Schematic of inactivation of PV-Arch interneurons during induction. A2) Decreased PV-IN spiking during inactivation (green) compared to control (black, *p<0.05, WSR, n=5). B1) PV-IN inactivation enhanced PN depolarization during TBS (green vs. black trace). B2) PN firing rates during induction with PV-IN (blue) or SST-IN (magenta) inactivation or VIP-IN activation (green). C1) Normalized EPSP amplitude with PV-IN inactivation (blue) or inactivation plus APV (black). C2) Enhancement of EPSP amplitude 25-30 min post induction (blue trace, filled circles) compared to baseline (black trace, open circles, **p: 0.003, paired t-test). C3) Normalized EPSP amplitude (**p: 0.004) and area (**p: 0.004, 1 sample t-test) were >1. D1) Normalized EPSP amplitude in two conditions- 1) inhibition intact and evoked backpropagating APs in the PN during induction (FR>5 Hz, gray triangles, n=6) and 2) PV-IN inactivation and PN FR <2 Hz during induction (open blue circles, n=8). D2) Normalized EPSP amplitude 25-30 min post induction with PV-IN inactivation for low PN FR (<2Hz, open circles), high PN FR (>5Hz, solid circles,* p: <0.05) or evoked backpropagation (BP>5Hz, gray triangles,* p: <0.05, WSR). D3) Normalized EPSP amplitude 25-30 min post induction (left axis) conditioned on <2 Hz FR in PNs (right axis, squares). Shown for PV-IN inactivation (open blue circles), SST-IN inactivation, (solid magenta, * p: <0.05, WSR) or VIP-IN activation (green circles,* p: <0.05, WSR). Average FR shown for each group (right axis, mean+/- SD, squares).